https://doi.org/10.5194/amt-2024-80
Preprint. Discussion started: 11 June 2024


Atmospheric Measurement Techniques Discussions

# Observed impact of the GNSS clock data rate on Radio Occultation bending angles for Sentinel-6A and COSMIC-2

Sebastiano Padovan[1], Axel Von Engeln[1], Saverio Paolella[1], Yago Andres[1], Chad R. Galley[2], Riccardo Notarpietro[1], Veronica Rivas Boscan[1], Francisco Sancho[1], Francisco Martin Alemany[1], Nicolas Morew[1], and Christian Marquardt[1]

[1]European Organisation for the Exploitation of Meteorological Satellites, Darmstadt 64295, Germany
[2]Jet Propulsion Laboratory, California Institute of Technology, Pasadena, CA 91109, USA

**Correspondence:** S. Padovan (sebastiano.padovan@external.eumetsat.int)

**Abstract.**

Space-based Radio Occultation (RO) experiments currently require the tracking of signals from the Global Navigation Satellite System (GNSS) by a Low-Earth-Orbit (LEO) satellite as the signals travel through different layers of the atmosphere. The orbit and clock solutions for the GNSS constellations affect these experiments in two ways: They are needed to obtain a zero-differencing GNSS-based orbit and clock solution for the LEO, and they enter directly the processing of each single radio occultation profile, where the orbit and clock information for the transmitter (GNSS satellite) and receiver (LEO) is required. In this work, we investigate how different GLONASS and GPS orbit and clock solutions affect the statistical properties of RO profiles by comparing our results with forward-modelled bending angle profiles obtained from the European Centre for Medium-Range Weather Forecasts (ECMWF) short-range forecasts. Given that GNSS orbits are relatively smooth, the focus will be on the effect of different transmitter clock data rates, and we tested the range from 1 to 30 seconds. The analysis is based on the reprocessing of Sentinel-6A data (four months in 2021, or about 110k occultations) and of a smaller sample of recent COSMIC-2/FORMOSAT-7 data (about 9k occultations). We find that at impact heights above about 35 km GLONASS bending angles statistics markedly improve with the use of high-rate clock information. For GPS, not much is gained by using rates higher than 30 s, and the statistics are better for more recent GPS blocks. These results are likely the manifestation of the different short-timescale behaviour of the atomic clocks onboard the GPS and GLONASS constellations.

## 1 Introduction

The estimation of bending angle (BA) profiles of signals from the Global Navigation Satellite System (GNSS) travelling between a GNSS satellite and a Low-Earth-Orbit (LEO) spacecraft through the Earth's atmosphere requires an accurate knowledge of the position, velocity and clock of the two space vehicles. In the Radio Occultation (RO) processing described in this work, the GNSS positions and clocks are provided as auxiliary files. They are used explicitly in the computation of each BA (through, e.g., the Doppler equation, Kursinski et al., 1997) and implicitly, given that they are required to obtain the LEO orbit and receiver clock solutions.

https://doi.org/10.5194/amt-2024-80
Preprint. Discussion started: 11 June 2024


Atmospheric Measurement Techniques Discussions

The GNSS space vehicles have revolution periods in excess of 10 hours and their orbits, which are largely controlled by gravitational dynamics, are relatively smooth and are typically provided at a rate of few minutes. The GNSS clocks are needed to synchronize the receiver clock when performing the LEO Precise Orbit Determination (POD). Being GNSS atomic clocks affected by random stochastic noises, a smaller sampling interval is required to obtain accurate interpolations, as needed by the bending-angle-retrieval process. As a reference, the Center for Orbit Determination Europe (CODE) currently provides orbits and clocks with a 5 min and a 30 s sampling rate, respectively, for rapid products (latency of 18 hours, Dach et al., 2023b) and 5 min and 5 s sampling rate for orbits and clocks for final products (latency of two weeks, Dach et al., 2023a). The Jet Propulsion Laboratory (JPL) Global Differential GPS (GDGPS, www.gdgps.net) real-time (RT) GNSS products are available with a 1 min orbit sampling and a 1 s clock sampling (https://cddis.nasa.gov/archive/gnss/products/realtime, https://sideshow.jpl.nasa.gov/pub/JPL_GNSS_Products/RealTime).

RO represents a high-rate application of GNSS products, since a typical radio occultation event has a duration of few minutes at most. At these time intervals, different GNSS constellations and different clock hardware within a given constellation show a range of clock stabilities (e.g., Hauschild et al., 2013; Griggs et al., 2015). These stability analyses are based on some form of the Allan Deviation, and point to the need, for the more unstable GNSS clock hardware, for high-rate corrections in order to obtain high-quality BA products.

The analysis of Sentinel-6A (S6A) RO data performed at the European Organisation for the Exploitation of Meteorological Satellites (EUMETSAT) using different GNSS data streams provided the motivation for this study (section 2). The experiment set-up is described in section 3. The bulk of the analysis is based on a 4-month-long batch of data from the S6A RO experiment (section 4.1) and it is complemented by a smaller batch of COSMIC-2/FORMOSAT-7 data (section 4.2). Discussion and conclusions are in section 5.

## 2 Motivation

The S6A spacecraft is the latest member of the family of altimetry reference missions (e.g., Donlon et al., 2021). For the first time, such a mission has been equipped with an RO instrument, which has been built by JPL (see also Paolella et al., 2024, this issue). The receiver is connected to a POD antenna, which tracks only GPS signals, and to two occultation antennas tracking both GPS and GLONASS signals, located in the velocity and anti-velocity direction. The entire mission is operated by EUMETSAT. For the RO experiment, JPL is responsible for the provision of Near-Real Time (NRT) RO data, while EUMETSAT for Non-Time Critical (NTC) RO products. These two operational streams are based on the same level zero data, received by EUMETSAT from the spacecraft through its ground segment and redistributed to JPL. JPL is one of the analysis centers of the international GNSS service (IGS) and, through an operational agreement, provides the auxiliary GNSS data for both RO data streams. The NTC data stream has a formal timeliness of 60 days, but it is kick-started as soon as the GNSS auxiliary data are available. Typically, EUMETSAT receives this data within two weeks from sensing time.

In addition to the operational NTC processor (referred to also as OPE processor), for monitoring purposes, at EUMETSAT we deployed an offline Short-Time Critical (STC) processor, which uses the CODE rapid products as GNSS auxiliary data

https://doi.org/10.5194/amt-2024-80
Preprint. Discussion started: 11 June 2024


Atmospheric Measurement Techniques Discussions

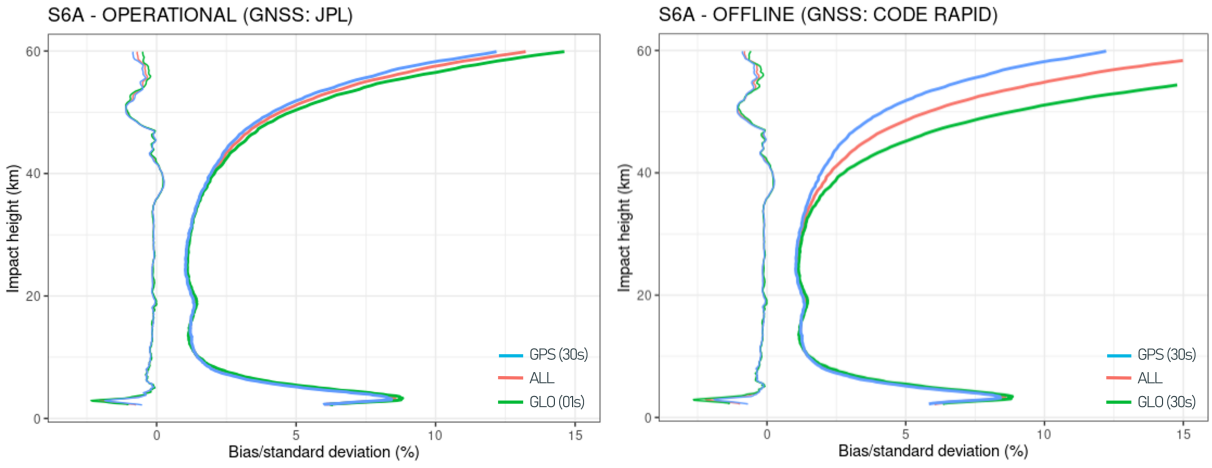


**Figure 1.** Sentinel-6A robust statistics against ECMWF short-range forecasts for two data sets for the period Feb 24$^{th}$-Mar 31$^{st}$, 2024, corresponding to about 38k single bending angle profiles for each set. **Left**: Operational data stream, where the POD is based on Bernese 5.2 (Section 3.1) and the GNSS auxiliary data are from JPL, with 30 s and 1 s clock rate for GPS and GLONASS, respectively. **Right**: STC offline data stream, where the POD is based on Bernese 5.4 (Section 3.1) and the GNSS auxiliary data are CODE rapid products, with clocks at 30 s for both GPS and GLONASS.

(Dach et al., 2023b), thus having a timeliness of about 24 hours. As part of this monitoring activity, for both the offline-STC and the operational-NTC processors, robust statistics are computed for the bias and standard deviation with respect to the forward-modelled bending angle profiles extracted by the European Centre for Medium-Range Weather Forecasts (ECMWF) short-range forecasts. The comparison of the statistics between the STC and OPE data streams provides a first indication of the importance of the GNSS clock data rate in the quality of the derived RO products. In Figure 1 we plot the bias and the standard deviation for both the OPE and the STC processor, using recent data from the period between February 24$^{th}$ and March 31$^{st}$, 2024, which corresponds to about 38k individual bending angle profiles per processor. The bias profiles between the two processors and for the two constellations are self-consistent and hardly distinguishable. For the standard deviation, the situation is different. Both for STC and for NTC the GPS clock products have a 30 s sampling rate. The different data source–CODE rapid for the STC and JPL final for the OPE–does not affect the overall standard deviation for GPS. For GLONASS, the STC processor uses the CODE rapid 30 s clocks, while the OPE processor is fed with 1 s JPL RT clock products. Above about an impact height of 35 km, the GLONASS standard deviation curves (green) are markedly different. Previous work has pointed out the lesser short-term stability of GLONASS clocks with respect to GPS ones, at least starting with Block IIF satellites (Griggs et al., 2015; Hauschild et al., 2013). Less stable clocks would require a higher rate correction to compensate its noise, and the results of Figure 1 point into this direction.

Given that the work of Hauschild et al. (2013) and Griggs et al. (2015) is several years old, and both the GPS and GLONASS constellations have been evolving in the meantime, we show in Figure 2 the modified Allan Deviation (e.g., Griggs et al., 2015) for the 1 s JPL RT clock products for December 31$^{st}$, 2021, a date which is part of the main S6A processing campaign below

https://doi.org/10.5194/amt-2024-80
Preprint. Discussion started: 11 June 2024


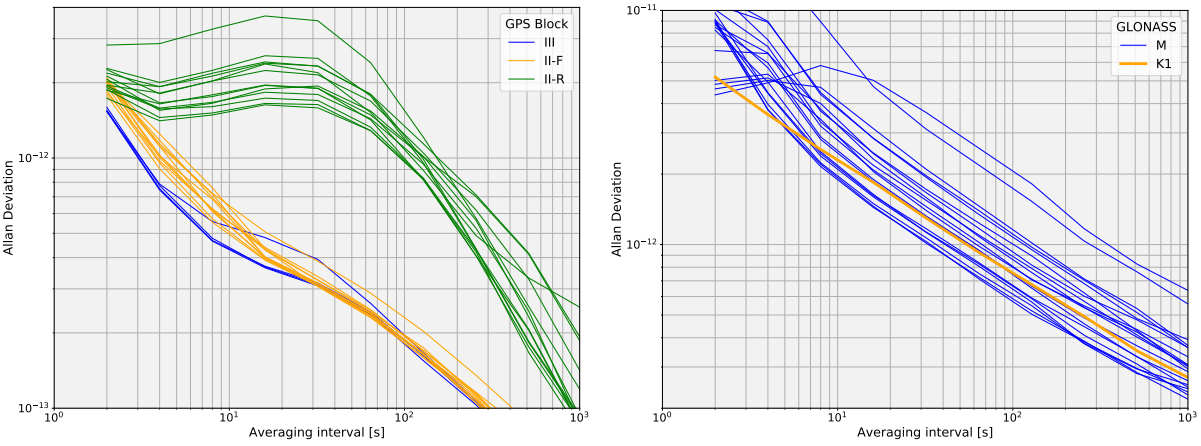


**Figure 2.** Modified Allan Deviation for the GPS (left) and GLONASS (right) constellations for December 31st, 2021, calculated using JPL real-time 1 s clock data. Please note the different range of the y-axis.

(Section 4.1). At that time in the GPS constellation there were 15, 12 and 5 Block II-R, Block II-F and Block III satellites, respectively. The results for the GPS satellites are similar to those of figure 7 of Griggs et al. (2015), with the addition of the group of Block III satellites, which show a better performance on the short timescales (< 10 s), and are similar to the Block II-F between $10^1$ and $10^2$ seconds. The GLONASS constellation was almost completely composed by GLONASS-M satellites, with a single GLONASS-K1, which displays a slight better performance at the very short timescales.

## 3 Set-up of the experiments

Unless otherwise noted, all the experiments described below are based on the re-processing of radio occultation data from level zero up to BA. We processed S6A and COSMIC-2/FORMOSAT-7 data, which have the same RO receiver type. The level zero data is decoded using a JPL-provided software compliant with the International Traffic in Arms Regulations (ITAR). The RO processing is performed with the EUMETSAT-developed and -maintained Yet Another Radio Occultation Software (YAROS), and detailed information on the processing approach can be found in Paolella et al. (2024). Here, we provide some details on the POD processing setup and on the employed GNSS auxiliary data.

### 3.1 POD

The LEO orbit and clock solutions are obtained with the latest version of the Bernese GNSS software (BSW5.4) using zero-differenced GNSS data (Jäggi et al., 2007; Bock et al., 2011). BSW5.4 allows for the modeling of non-gravitational forces on the LEO, namely air-drag and direct and reflected radiation pressure (Mao et al., 2019). To make use of these models, a representation of the shape of the spacecraft is required. In our simulations we use a macro model for S6A based on Montenbruck et al. (2021), but no shape model is employed for COSMIC-2. BSW5.4 has the capability of performing zero-differencing inte-

https://doi.org/10.5194/amt-2024-80
Preprint. Discussion started: 11 June 2024


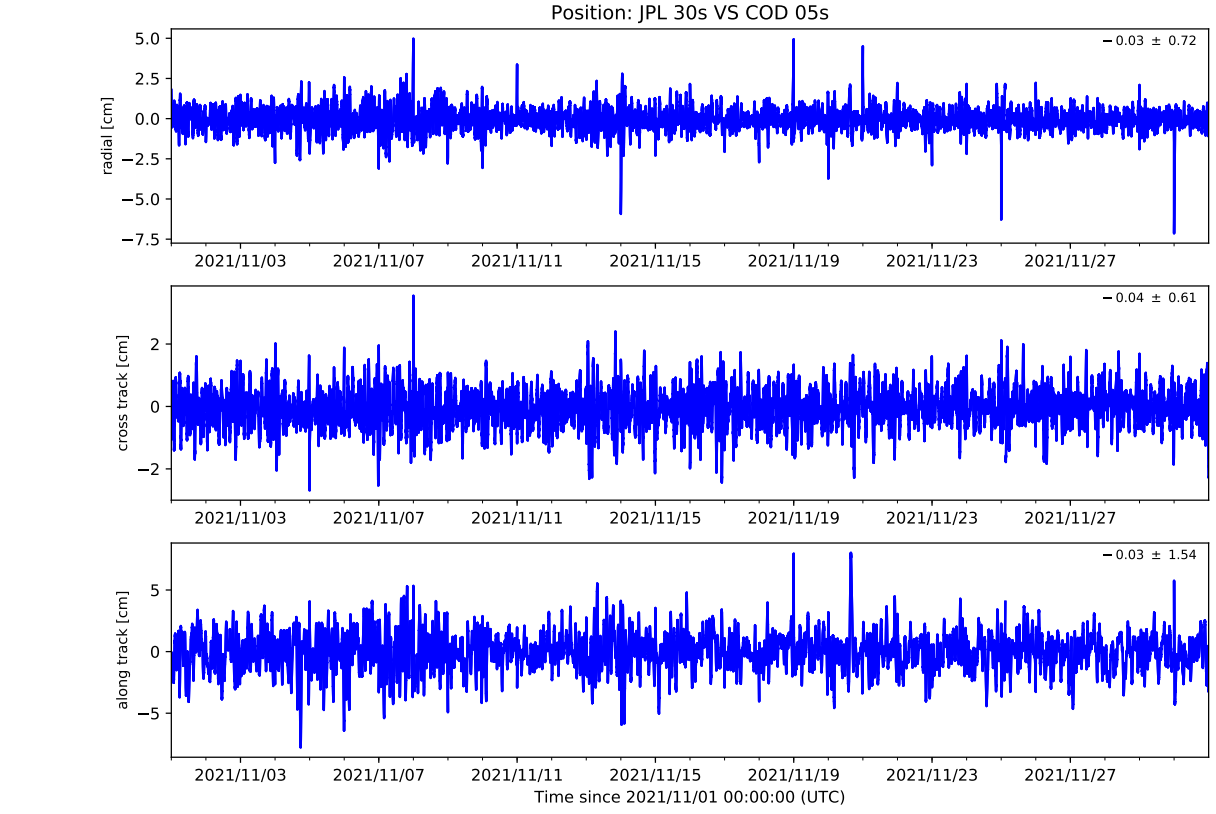


**Figure 3.** Comparison along the radial (top), cross track (middle) and along track (bottom) directions of two S6A orbit solutions for the month of November 2021. In each panel the mean ± the root mean square (RMS) is indicated. The two solutions are obtained with the same software (Bernese 5.4) but with two different GNSS auxiliary data products: JPL real-time GPS (15 min orbits and 30 s clocks) and CODE final GPS (5 min orbits and 5 s clocks).

ger ambiguity resolution using the Bias-SINEX products (Villiger et al., 2019; Schaer et al., 2021). However, these products are not part of the operational agreement with JPL and our solutions are based on the float-ambiguity resolution approach. Integer-ambiguity fixing has been shown to be better than the float-ambiguity approach (e.g., Montenbruck et al., 2018). However, the use of the float ambiguity solution in the BA processor is enough for generating high-quality RO products (e.g., Kursinski et al., 1997; Montenbruck et al., 2008; Innerkofler et al., 2020). The POD software currently embedded in the operational processor is Bernese version 5.2 (BSW5.2), which has neither the non-gravitational force models nor the zero-differenceing ingeter-ambiguity-resolution algorithms available.

https://doi.org/10.5194/amt-2024-80
Preprint. Discussion started: 11 June 2024


Atmospheric Measurement Techniques Discussions

We assess the quality of a given POD solution in several complementary ways. There is an internal quality assessment within Bernese, where the final so-called reduced-dynamic orbit is compared to the kinematic orbit solution. (A reduced-dynamic orbit indicates an orbit solution where the dynamical forces, originating, e.g., from the extended gravitational field of the Earth, from the Sun, etc. are taken into account. The model cannot realistically take into account all possible forces, hence "reduced", and some empirical parameters compensate for this. See., e.g., Montenbruck et al., 2005, and references therein.) Since both the reduced-dynamic and the kinematic orbit are based on data from the same sensor, and the data handling component is common, their comparison cannot detect any problem originating from, e.g., an error in the attitude modeling or in the definition of the position of the POD antenna. Thus, we also use a different POD software, the NAvigation Package for Earth Observation Satellites (NAPEOS, Springer et al., 2011), to crosscheck the consistency of the BSW-based reduced-dynamic solution with the NAPEOS-based solution. As a result of being an altimetry reference mission, in addition to the RO POD antenna (RO-POD), S6A also features another POD antenna (GNSS-POD) with a completely separate receiver and ultra-stable oscillator (e.g., Donlon et al., 2021). The comparison of the GNSS-POD solution with the RO-POD solution provides a receiver-independent way to crosscheck the solution (of course the clock solution in this case cannot be compared, given that the two receivers have different oscillators). Furthermore, the GNSS-POD-based solution itself is routinely compared with solutions obtained by the members of the Copernicus POD quality working group (Fernández et al., 2024), which EUMETSAT is part of. The above checks allow to perform several complementary S/W-, receiver-, and processing-center-independent cross comparisons to validate our solution. Typically, the spread of the different orbits in the three-dimensional root mean square (3D-RMS) space is below 3 cm.

The focus of this work is to investigate the effect of different GNSS clock data rates on the RO BAs (see, e.g., Figure 1) and the effect is both direct, since they enter explicitly in the processing of each single RO profile, and indirect through their influence on the POD solution (section 1). In Figure 3 we compare two S6A solutions for the month of November 2021 (which falls within our main test campaign, see Section 4.1). One is obtained using JPL RT GPS products with clocks at 30 seconds and orbits at 15 minutes, the other using CODE final products with clocks at 5 seconds and orbits at 5 minutes. The RINEX observation files, decoded from level zero data provided by the RO receiver at the rate of 1 s, are downsampled to 30 s when using JPL products and to 10 s when using CODE products. With 5 s clocks, one could also employ 5 s RINEX data, but it has been shown that not much is gained in this case, and the GNSS-POD receiver provides data at the rate of 1 and 10 seconds for carrier-phase and pseudo-range, respectively (Fernández et al., 2024). In the POD processing, using a RINEX data rate higher than the clock data rate of the GNSS products would not be beneficial, but would rather increase the noise of the solution (Dach et al., 2015). It is clear from the figure that there is a good agreement between the two solutions, with biases below the millimeter level and RMS below the 2 centimeter in any given direction. The comparison for the velocity solution (not shown) is even better, with both biases and RMS below 0.01 mm/s. These results are well within the standard target specifications of 5 cm and 0.05 mm/s for RO missions (e.g., Innerkofler et al., 2020).

https://doi.org/10.5194/amt-2024-80
Preprint. Discussion started: 11 June 2024


Atmospheric Measurement Techniques Discussions

### 3.2 GNSS auxiliary data

For the results presented in the next section, the GNSS auxiliary data that we employ are JPL RT data, with one second clocks, 15 minutes orbits, and daily earth rotation parameters. The orbit and rotation products are not modified. Different sets of GNSS auxiliary data are created by modifying the clock products. We use a straightforward downsampling (i.e., decimation) of the clocks to create four additional sets of clock products with rates of 2, 5, 10, and 30 seconds. Another obvious approach would be to first fit the data of the 1 s product before downsampling it. Using a fit would be more stable against outliers. For example, if every 30$^{th}$ data point were an outlier, the 30 s downsampled product would contain little useful information. With this caveat in mind, the direct decimation represents a conservative choice since it could increase the relative percentage of outliers, thus adding to the loss of information in the downsampled products.

## 4 Results

Given the self-consistency of POD solutions obtained using different GNSS products (Figure 3), the focus of this section is on the effects of using different GNSS clock data rate in the BA data processing. The GNSS transmitter clock bias plays an important role when processing the reconstructed signal phases (i.e., the ones obtained by the level zero decoder) with a zero-differencing algorithm (e.g., Langley et al., 2017). The main test uses S6A data, and a validation test is performed using COSMIC-2.

For all the experiments presented in this section, the POD solution for the LEO has been obtained using JPL GPS RT data (the POD antenna only tracks the GPS constellation) with a clock downsampled to 30 s and, correspondingly, a RINEX at 30 s (Section 3.1). For the RO processing each GNSS auxiliary data set has the same orbits and earth rotation parameters. Five different sets are used, corresponding to differences in the data rate of the clock products as illustrated in Section 3.2.

### 4.1 Sentinel 6A

We processed four months of S6A data, from September 1$^{st}$ to December 31$^{st}$, 2021, which corresponds to around 110k occultation profiles. The results on the bias and standard deviation against ECMWF forward-modelled profiles are presented per constellation, following the approach of Figure 1.

Figure 4 shows that while the bias is unaffected by the use of different GLONASS clock data rates (in the 1 s–30 s range), the standard deviation markedly improves for impact heights above about 35 km. At 40 km the standard deviation decreases by about 1% going from a 30 second to a 1 second clock product. Using 30 s GLONASS clocks a 5% standard deviation is reached at an impact height of about 45 km, while with a 1 s clock this occurs at about 52 km.

Figure 5 shows that, as it is the case for the GLONASS occultations, the robust bias for the GPS occultations is practically unaffected by the different GPS clock data rates employed. Unlike GLONASS, though, the standard deviation only shows a minor dependence on the GPS clock data rate. However, as visible in the standard deviation at high impact heights (Figure 5, right panel), there is not a clear trend in the standard deviation with the increasing clock data rate, contrary to the case of

https://doi.org/10.5194/amt-2024-80
Preprint. Discussion started: 11 June 2024


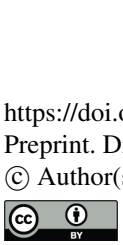

Atmospheric Measurement Techniques Discussions

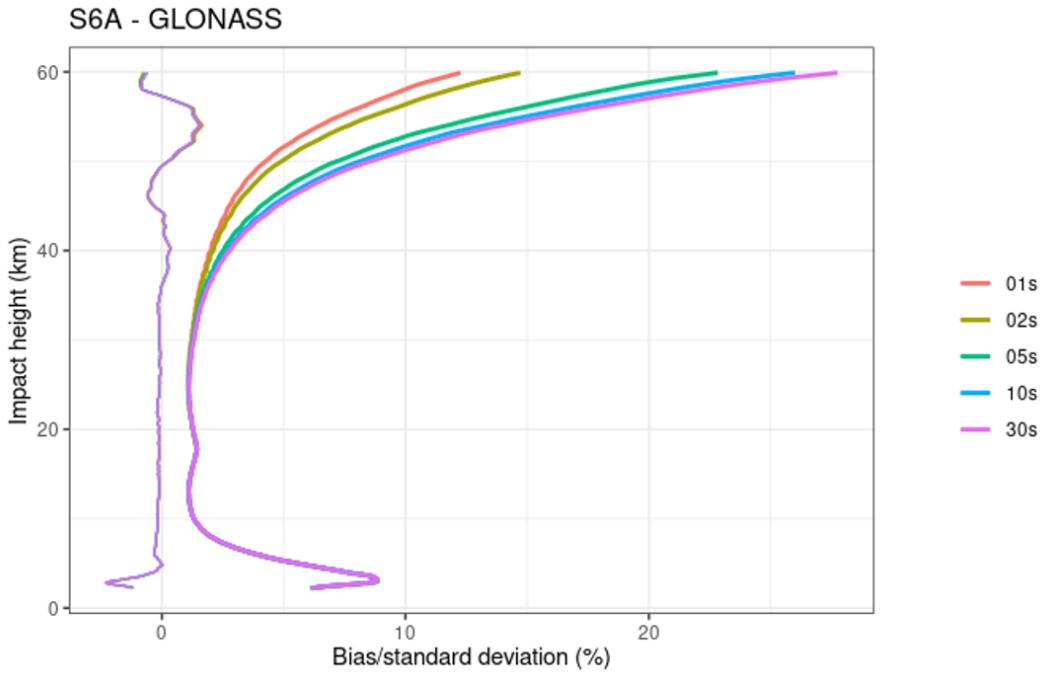


**Figure 4.** Robust statistics of S6A GLONASS occultations against ECMWF short-range forecasts. Each set corresponds to bending angle profiles processed with different GLONASS clock data rates, as indicated in the legend. Above an impact height of about 35 km, there is a clear advantage in using high rate GLONASS clocks.

GLONASS (Figure 4). Given that the clock behaviour of the GPS constellation shows a block dependence (Figure 2), we also plot the bias and standard deviation curves at high impact heights for the different GPS blocks separately (Figure 6). Overall, for a given clock data rate, the standard deviation improves going from Block-IIR, to Block-IIF and to Block-III. However, for a given Block, the effect of increasing the GPS clock data rate does not affect the standard deviation curve consistently. For the Block-III (Figure 6, right), going from 30 s to 1 s clocks brings a steady increase in the standard deviation at a given height, with the effect being really minor between 30 and 5 seconds, but becoming noticeable with 2 and 1 second clocks. For the Block-IIF (Figure 6, middle), all sets are mostly coincident, with a slight degradation of the standard deviation when using the 1 second clock. For the Block-IIR (Figure 6, left), increasing the clock data rate improves the standard deviation. The improvement is steady in going from 30 to 5 seconds. The 2 and 5 seconds curves coincides, while going to a rate of 1 second increases the standard deviation.

### 4.2 COSMIC-2

To verify the results observed using S6A data, we used data from COSMIC-2 (e.g., Ho et al., 2020) in a smaller-scale test using three days in 2023 (August 5$^{th}$–7$^{th}$), which corresponds to about 9200 occultations. As was the case for S6A, the increase in

https://doi.org/10.5194/amt-2024-80
Preprint. Discussion started: 11 June 2024


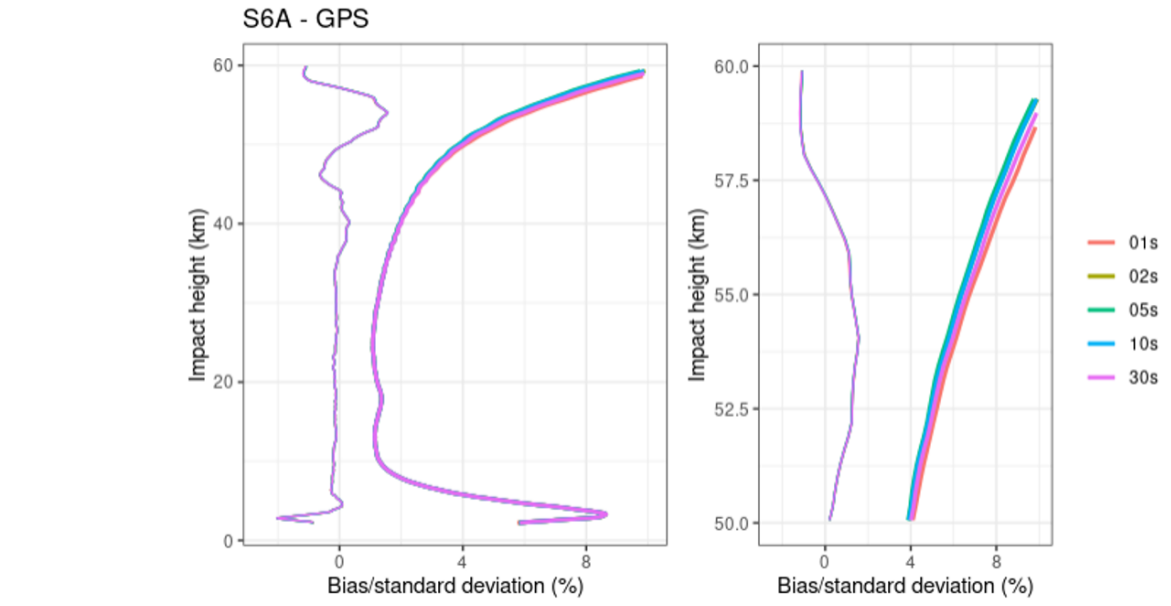


**Figure 5.** Robust statistics of S6A GPS occultations against ECMWF short-range forecasts. Each set corresponds to bending angle profiles processed with different GPS clock data rates, as indicated in the legend. Unlike the case of S6A GLONASS occultations (Figure 4), the standard deviation is largely unaffected by the GPS clock data rate used, as seen in the right panel, which is a zoomed-in view of the 50-60 km impact height range.

the clock data rate for GLONASS occultations improves the standard deviation with minor effects on the bias (Figure 7). For GPS occultations we only used GPS clocks at 30 seconds, and the results for the standard deviation are consistent with what was found with S6A, where there is an improvement in going from Block-IIR, to Block-IIF, to Block-III (Figure 8).

## 5 Discussion and Conclusions

The analysis performed in this work points at the importance of using high-rate GLONASS clock data to obtain the best performance in terms of standard deviation at impact heights in excess of 35 km, with improvements observed up to 1 s, which is the highest rate tested (Figures 1, 4 and 7). Even though more work is needed to elucidate the variation of the standard deviation curves for the GPS constellation as a function of the clock data rate (Figure 6), the 30 s clock products provide comparable performance to the GLONASS 1 s products (Figures 1, 5 and 8). These results confirm expectations based on the analysis of GNSS clock noise at RO-relevant timescales (Harnisch et al., 2013; Griggs et al., 2015).

This work focused on GPS and GLONASS occultations recorded by the S6A and COSMIC-2 RO receivers. There is an ongoing effort to assess the impact of a large number of real RO observations on numerical weather predictions (NWPs), with the goal of verifying the conclusions of studies based on ensemble data assimilations (EDA, e.g., Harnisch et al., 2013) or observing system simulation experiments (OSSE, e.g., Privé et al., 2022). In the framework of this Radio Occultation Modeling

https://doi.org/10.5194/amt-2024-80
Preprint. Discussion started: 11 June 2024


Atmospheric Measurement Techniques Discussions

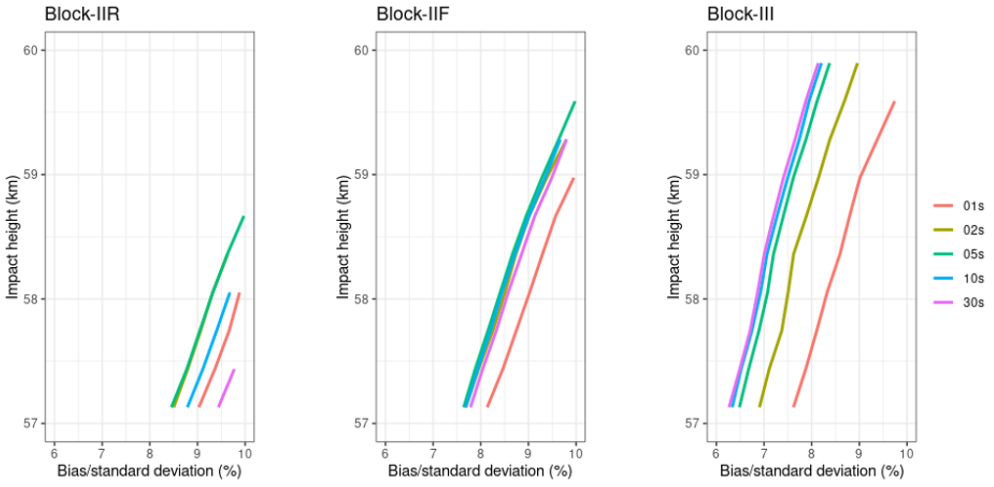


**Figure 6.** Above-50-km robust standard deviation of S6A GPS occultations against ECMWF short-range forecasts (as Figure 5, right panel), for different GPS clock data rates (legend) and hardware. Left: Block-IIR; Middle: Block-IIF; Right: Block-III. From left to right the standard deviation improves at any given clock data rate. However, for a given Block (i.e., panel), the effect of increasing the GPS clocks data rate is not unique.

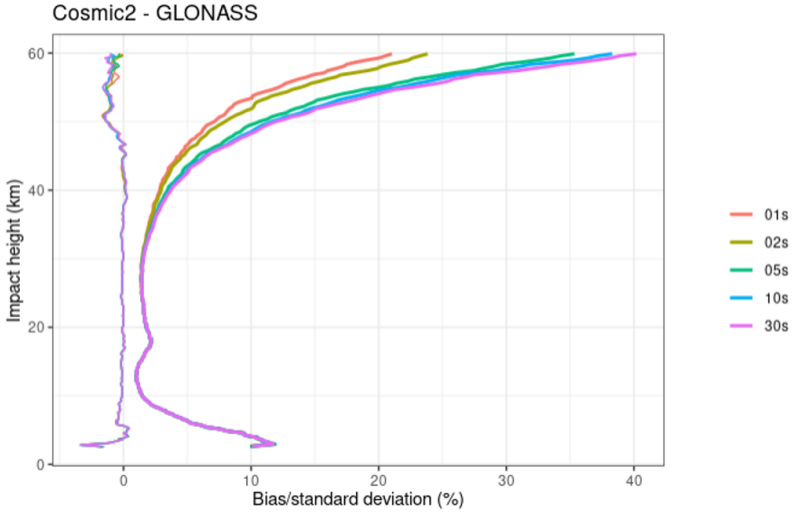


**Figure 7.** Robust statistics of COSMIC-2 GLONASS occultations against ECMWF short-range forecasts. Each set corresponds to bending angle profiles processed with different GLONASS clock data rates, as indicated in the legend. Above an impact height of about 35 km, there is a clear advantage in using high rate GLONASS clocks, as was the case for S6A (Figure 4).

Experiment (ROMEX, McHugh et al., 2023; Anthes et al., 2024), about 30k occultations per day for a period of three months
190 in 2022 will be made available to the science community at large, mostly from level zero (Anthes et al., 2024). This trove of

https://doi.org/10.5194/amt-2024-80
Preprint. Discussion started: 11 June 2024


Atmospheric Measurement Techniques Discussions

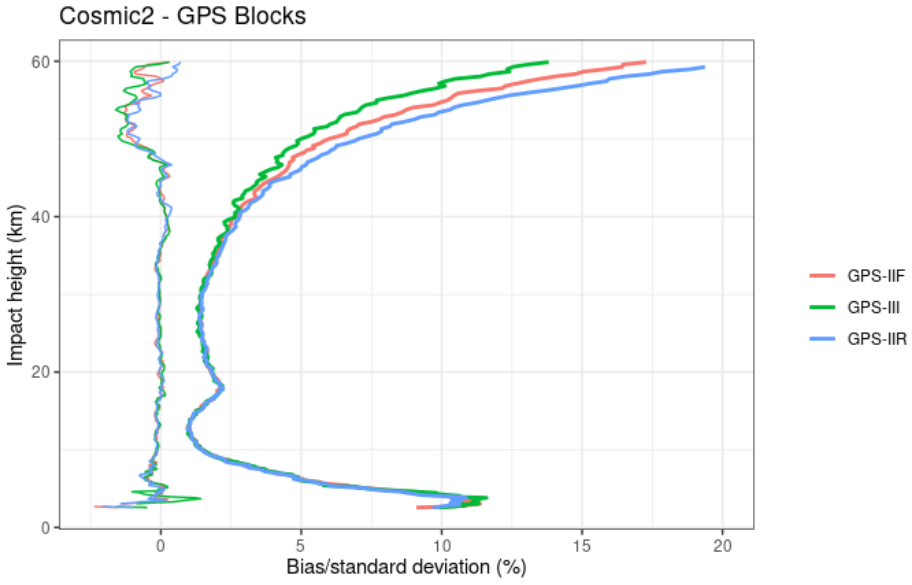


**Figure 8.** Robust statistics of COSMIC-2 GPS occultations against ECMWF short-range forecasts, obtained using 30 s GPS clock products. Each set corresponds to a different GPS Block, as indicated in the legend. As was the case for S6A for a given clock data rate (Figure 6), Block-III is better than Block-IIF, which is in turn better than Block-IIR.

data could be used to further extend the analysis performed here to include Galileo and Beidou occultations and other receiver types.

For RO observations, the best combination of accuracy and small uncertainty is expected in the 5 to 30 km range, the so-called RO sweet-spot (Kursinski et al., 1997), and our results (Figures 1, 4, 5, 7, 8) provide yet another confirmation of this expectation (e.g., Anthes et al., 2022, and references therein). Recently, RO observations have been included as key observations in the assessment of temperature trends in the upper troposphere and lower stratosphere (Masson-Delmotte et al., 2021, Figure TS. 10, pg. 70). Given that GLONASS high-rate clock data clearly improves the uncertainty, RO processing centers should aim at using this type of products, given their potential impact on both NWPs (Lonitz et al., 2021) and climate studies (Gleisner et al., 2022).

## Competing interests

The contact author has declared that none of the authors has any competing interests.

https://doi.org/10.5194/amt-2024-80
Preprint. Discussion started: 11 June 2024

Atmospheric Measurement Techniques Discussions

**Acknoledgements**

The research conducted by C.R.G. was carried out at the Jet Propulsion Laboratory, California Institute of Technology, under a contract with the National Aeronautics and Space Administration (80NM0018D0004).

https://doi.org/10.5194/amt-2024-80
Preprint. Discussion started: 11 June 2024


Atmospheric Measurement Techniques Discussions

## References

Anthes, R., Sjoberg, J., Feng, X., and Syndergaard, S.: Comparison of COSMIC and COSMIC-2 Radio Occultation Refractivity and Bending Angle Uncertainties in August 2006 and 2021, Atmosphere, 13, https://doi.org/10.3390/atmos13050790, 2022.

Anthes, R. A., Marquardt, C., Ruston, B., and Shao, H.: Radio Occultation Modeling Experiment, Bull. Am. Met. Soc., in revision, 2024.

Bock, H., Jäggi, A., Meyer, U., Visser, P., van den IJssel, J., van Helleputte, T., Heinze, M., and Hugentobler, U.: GPS-derived orbits for the GOCE satellite, J. Geod., 85, 807–818, https://doi.org/10.1007/s00190-011-0484-9, 2011.

Dach, R., Lutz, S., Walser, P., and Fridez, P., eds.: Bernese GNSS Software Version 5.2. User Manual, University of Bern, Bern Open Publishing, Bern, https://doi.org/10.7892/boris.72297, 2015.

Dach, R., Schaer, S., Arnold, D., Brockmann, E., Kalarus, M. S., Prange, L., Stebler, P., and Jäggi, A.: CODE final product series for the IGS, https://doi.org/10.48350/185744, 2023a.

Dach, R., Schaer, S., Arnold, D., Brockmann, E., Kalarus, M. S., Prange, L., Stebler, P., and Jäggi, A.: CODE rapid product series for the IGS, https://doi.org/10.48350/185740, 2023b.

Donlon, C. J., Cullen, R., Giulicchi, L., Vuilleumier, P., Francis, C. R., Kuschnerus, M., Simpson, W., Bouridah, A., Caleno, M., Bertoni, R., Rancaño, J., Pourier, E., Hyslop, A., Mulcahy, J., Knockaert, R., Hunter, C., Webb, A., Fornari, M., Vaze, P., Brown, S., Willis, J., Desai, S., Desjonqueres, J.-D., Scharroo, R., Martin-Puig, C., Leuliette, E., Egido, A., Smith, W. H., Bonnefond, P., Le Gac, S., Picot, N., and Tavernier, G.: The Copernicus Sentinel-6 mission: Enhanced continuity of satellite sea level measurements from space, Remote Sens. Env., 258, 112 395, https://doi.org/https://doi.org/10.1016/j.rse.2021.112395, 2021.

Fernández, J., Peter, H., Fernández, C., Berzosa, J., Fernández, M., Bao, L., Ángel Muñoz, M., Lara, S., Terradillos, E., Féménias, P., and Nogueira, C.: The Copernicus POD Service, Adv. Space Res., https://doi.org/https://doi.org/10.1016/j.asr.2024.02.056, 2024.

Gleisner, H., Ringer, M. A., and Healy, S. B.: Monitoring global climate change using GNSS radio occultation, Climate and Atmospheric Science, 5, 6, https://doi.org/10.1038/s41612-022-00229-7, 2022.

Griggs, E., Kursinski, E. R., and Akos, D.: Short-term GNSS satellite clock stability, Radio Sci., 50, 813–826, https://doi.org/10.1002/2015RS005667, 2015.

Harnisch, F., Healy, S. B., Bauer, P., and English, S. J.: Scaling of GNSS Radio Occultation Impact with Observation Number Using an Ensemble of Data Assimilations, Monthly Weather Rev., 141, 4395 – 4413, https://doi.org/10.1175/MWR-D-13-00098.1, 2013.

Hauschild, A., Montenbruck, O., and Steigenberger, P.: Short-term analysis of GNSS clocks, GPS Sol., 17, 295–307, https://doi.org/10.1007/s10291-012-0278-4, 2013.

Ho, S.-P., Zhou, X., Shao, X., Zhang, B., Adhikari, L., Kireev, S., He, Y., Yoe, J. G., Xia-Serafino, W., and Lynch, E.: Initial Assessment of the COSMIC-2/FORMOSAT-7 Neutral Atmosphere Data Quality in NESDIS/STAR Using In Situ and Satellite Data, Remote Sens., 12, https://doi.org/10.3390/rs12244099, 2020.

Innerkofler, J., Kirchengast, G., Schwärz, M., Pock, C., Jäggi, A., Andres, Y., and Marquardt, C.: Precise Orbit Determination for Climate Applications of GNSS Radio Occultation including Uncertainty Estimation, Remote Sens., 12, https://doi.org/10.3390/rs12071180, 2020.

Jäggi, A., Hugentobler, U., Bock, H., and Beutler, G.: Precise orbit determination for GRACE using undifferenced or doubly differenced GPS data, Adv. Sp. Res., 39, 1612–1619, https://doi.org/10.1016/j.asr.2007.03.012, 2007.

Kursinski, E. R., Hajj, G. A., Schofield, J. T., Linfield, R. P., and Hardy, K. R.: Observing Earth's atmosphere with radio occultation measurements using the Global Positioning System, J. Geophys. Res. Atmospheres, 102, 23 429–23 465, https://doi.org/https://doi.org/10.1029/97JD01569, 1997.

https://doi.org/10.5194/amt-2024-80
Preprint. Discussion started: 11 June 2024




Langley, R. B., Teunissen, P., and Montenbruck, O.: Introduction to GNSS, in: Springer Handbook of Global Navigation Satellite Systems, edited by Teunissen, P. and Montenbruck, O., chap. Introduction to GNSS, pp. 3–23, Springer International Publishing, https://doi.org/10.1007/978-3-319-42928-1_1, 2017.

Lonitz, K., Marquardt, C., Bowler, N., and Healy, S.: Final Technical Note of 'Impact assessment of commercial GNSS-RO data', https://doi.org/10.21957/wrh6voyyi, 2021.

Mao, X., Arnold, D., Kalarus, M., Padovan, S., and Jäggi, A.: GNSS-based precise orbit determination for maneuvering LEO satellites, GPS Sol., 27, 147, 2019.

Masson-Delmotte, V., Zhai, P., Pirani, A., Connors, S., Péan, C., Berger, S., Caud, N., Chen, Y., Goldfarb, L., Gomis, M., Huang, M., Leitzell, K., Lonnoy, E., Matthews, J., Maycock, T., Waterfield, T., Yelekçi, O., Yu, R., and Zhou, B., eds.: Climate Change 2021: The Physical Science Basis. Contribution of Working Group I to the Sixth Assessment Report of the Intergovernmental Panel on Climate Change, Cambridge University Press, Cambridge, United Kingdom and New York, NY, USA, https://doi.org/10.1017/9781009157896, 2021.

McHugh, M., Shao, H., Anthes, R., Ruston, B., Marquardt, C., and ROMEX members: Radio Occultation Modeling Experiment (ROMEX) Framework, White Paper, https://irowg.org/wpcms/wp-content/uploads/2023/05/ROMEX-Whitepaper-8-3-23.pdf, accessed on April 25, 2024, 2023.

Montenbruck, O., van Helleputte, T., Kroes, R., and Gill, E.: Reduced dynamic orbit determination using GPS code and carrier measurements, Aerosp. Sci. Techn., 9, 261–271, https://doi.org/https://doi.org/10.1016/j.ast.2005.01.003, 2005.

Montenbruck, O., Andres, Y., Bock, H., van Helleputte, T., van den Ijssel, J., Loiselet, M., Marquardt, C., Silvestrin, P., Visser, P., and Yoon, Y.: Tracking and orbit determination performance of the GRAS instrument on MetOp-A, GPS Sol., 12, 289–299, 2008.

Montenbruck, O., Hackel, S., and Jäggi, A.: Precise orbit determination of the Sentinel-3A altimetry satellite using ambiguity-fixed GPS carrier phase observations, J. Geod., 92, 711–726, https://doi.org/10.1007/S00190-017-1090-2, 2018.

Montenbruck, O., Hackel, S., Wermuth, M., and Zangerl, F.: Sentinel-6A precise orbit determination using a combined GPS/Galileo receiver, J. Geod., 95, 109, https://doi.org/10.1007/s00190-021-01563-z, 2021.

Paolella, S., Engeln, A. V., Padovan, S., Notarpietro, R., Marquardt, C., Sancho, F., Boscan, V. R., Morew, N., and Alemany, F. M.: Assessment of Operational Non-Time Critical Sentinel-6A Michael Freilich Radio Occultation Data: Insights into Tropospheric GNSS Signal Cutoff Strategies and Processor Improvements, Atm. Meas. Tech., 2024.

Privé, N. C., Errico, R. M., and Akkraoui, A. E.: Investigation of the Potential Saturation of Information from Global Navigation Satellite System Radio Occultation Observations with an Observing System Simulation Experiment, Monthly Weather Rev., 150, 1293 – 1316, https://doi.org/10.1175/MWR-D-21-0230.1, 2022.

Schaer, S., Villiger, A., Arnold, D., Dach, R., Prange, L., and Jäggi, A.: The CODE ambiguity-fixed clock and phase bias analysis products: generation, properties, and performance, J. Geod., 2021, https://doi.org/10.1007/s00190-021-01521-9, 2021.

Springer, T., Dilssner, F., Escobar, D., Flohrer, C., Otten, M., Svehla, D., and Zandbergen, R.: NAPEOS: The ESA/ESOC tool for Space Geodesy, in: EGU General Assembly, vol. 13, pp. EGU2011–8287, 2011.

Villiger, A., Schaer, S., Dach, R., Prange, L., Susnik, A., and Jäggi, A.: Determination of GNSS pseudo-absolute code biases and their long-term combination, J. Geod., 2019, https://doi.org/10.1007/s00190-019-01262-w, 2019.